UNIVERSIDAD COMPLUTENSE DE MADRID

FACULTAD DE CIENCIAS FÍSICAS

Máster Universitario en Astrofísica



TRABAJO DE FIN DE MÁSTER

Analysis of star formation in galaxies in filaments using the GAMA surveys

Análisis de la formación estelar en galaxias de filamentos usando el cartografiado GAMA

Paula Macías Pardo

Tutor/es:

Maritza A. Lara López

Jesús Gallego Maestro

Curso académico 2022-2023

Resumen

En el siguiente trabajo estudiamos el efecto del entorno sobre la morfología, la tasa de formación estelar (SFR) y la tasa de formación estelar específica (sSFR) a partir de una muestra de originalmente 192543 galaxias dentro de un rango de redshift de $0 < z < 0.213$ usando el cartografiado Galaxy and Mass Assembly (GAMA). Definimos una muestra control eliminando las galaxias en grupos y a partir de esta una posterior submuestra limitada en volumen para así controlar por efectos de selección. Se encuentran aumentos de la SFR de 0.108 y 0.042 dex en la relación M-SFR para galaxias en filamentos como señales cuantitativas del efecto del entorno. Respecto a la morfología, partimos de una distribución bimodal en el índice de Sérsic para las muestras completas de GAMA y filamentos en GAMA, con un 53% (GAMA) de las galaxias clasificadas como tipos tardíos y un 57% (filamentos) como tipos tempranos. Estas diferencias desaparecen cuando consideramos la muestra control y la limitada en volumen, poniendo de manifiesto la importancia del uso de este método para encontrar diferencias en propiedades estadísticas de muestras de galaxias.

Abstract

We study the environmental dependencies for morphology, star formation rate (SFR) and specific star formation rate (sSFR) from a original sample of 192543 galaxies within a redshift range of $0 < z < 0.213$ using the Galaxy And Mass Asssembly (GAMA) survey. We define a control sample by removing galaxies in groups, and a volume limited subsample to control for selection effects. We find SFR enhancements of about 0.108 and 0.042 dex in the M-SFR relation of filament galaxies which is a quantitative sign of an effect of the environment. Regarding the morphology, we find a bimodal distribution in the Sersic Index for the full GAMA and filaments in GAMA catalogs, with a 53% (GAMA) as late-type, and a 57% (filaments) as early-type galaxies. However, this difference disappear when the control and volume limited samples are considered, revealing the importance of using this methodology to find differences in statistical properties from galaxy samples.

Contents

1 Introduction: large-scale structure **1**

1.1 Galaxy and Mass Assembly survey (GAMA) 2

1.2 GAMA Galaxy group catalogue 3

2 Sample selection **4**

2.1 GANDALF catalog construction 4

2.2 BPT diagram 5

2.3 Errors estimation for the flux ratios used in the BPT diagram 7

2.4 Selection effects 8

2.5 Filaments and control sample 9

3 Star Formation Rate (SFR) **10**

3.1 Extinction and reddening estimation 11

3.2 Hα Star Formation Rates 12

3.3 Control sample and filaments 13

3.4 Volume limited subsample (V1) and filaments 14

3.5 Errors estimation for the SFR, sSFR 18

4 Morphology **19**

4.1 Control and V1 samples versus filaments 21

5 Summary and conclusions **22**

6 Future work **23**

References **24**

1. Introduction: large-scale structure

Galaxies are not spread out randomly across the Universe, they are arranged in the cosmic web which is composed of clusters and superclusters connected to each other by groups of galaxies. According to the density, galaxies can be classified as belonging to different types of regions: filaments, clusters, or voids. The properties of galaxies vary systematically as a function of environment which acts as determining to their fate and evolution. Regarding to the dark matter distribution, Sheth and Tormen (2004) find evidence that dark matter haloes of a given mass form earlier in dense regions and it has been found that other halo properties such as concentration and spin correlate with local environment. Hahn et al. (2007) investigated the redshift evolution of dark matter haloes properties in different large-scale structure environments and found that it influences the halo shape and formation time depending on the halo mass in relation to the typical mass scale of gravitational collapse at each redshift.

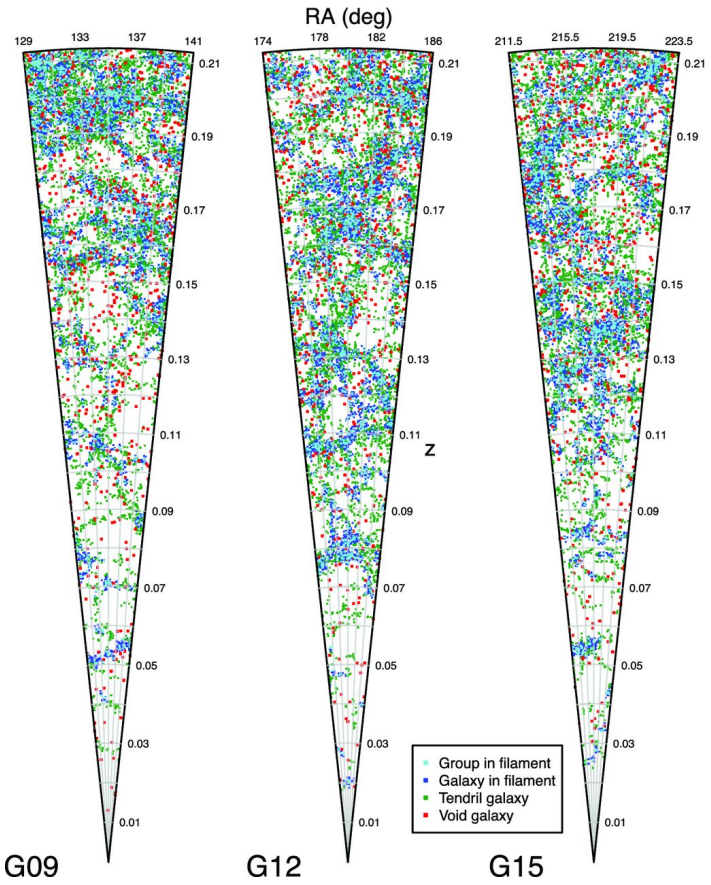


Figure 1: Galaxy distribution in the three GAMA regions, colour coded according to the environment classification given in Alpaslan et al. (2014). Groups in filaments, galaxies near filaments, galaxies in tendrils and void galaxies are shown in cyan, blue, green and red, respectively.

On the other hand, galaxy properties in the local Universe are known to vary systematically with environment. The morphological type of galaxies is earlier in the locally denser regions (morphology–density relation) (Avila-Reese 2007). Observational studies show that other properties besides morphology vary with environment: the galaxy property most sensitive to environment is specific star formation rate (sSFR) (Kauffmann et al. 2004), since the proximity of galaxies can often trigger dormant regions of gas into infall and galaxies in a dense environment are found to have suppressed star formation rates (Tanaka et al. 2004) from those of field galaxies. Other properties associated with star formation rate such as colour, stellar mass, gas content or luminosity function correlate strongly with local density. Different studies suggest that the origin of this relation could be a combination of initial cosmological conditions (nature) and external mechanisms that operate mostly in dense environments (nurture), such as ram-pressure and tidal stripping, galaxy harassment, strangulation or thermal evaporation of the disk gas, etc.

In the nature-nurture scenario driving galaxy evolution we focus on the nurture aspect, in particular we are concerned in determining whether a galaxy in a filament, in this case, is discernibly different from a field galaxy. Our understanding of large-scale structure ($\geq 1h^{-1}$Mpc) and its possible influence in galaxies evolution is developed thanks to simulations and galaxy surveys like the 2dFGRS, the MGC, the SDSS-DR7, the 6dFGS and GAMA. In this work, we use the large-scale structure classification for the three equatorial GAMA fields done by Alpaslan et al. (2014), shown in Figure 1. Their algorithm detect filaments of groups and galaxies as well as smaller structures known as tendrils and voids. Tendrils would correspond to coherent structures on a much smaller scale than filaments which are formed entirely by galaxies, whereas voids are less dense regions. The algorithm works on the basis of two assumptions: first, that all bright, high luminosity groups tend to live in knots of filaments and second, that void galaxies are only clustered at extremely small scales. The method to find filaments is based on a minimal spanning tree (MST) approach to groups of galaxies, instead of galaxies so that they pick out skeletal patterns and linear associations, detecting objectively large-scale structure in the Universe. Then, given a sample of groups and galaxies the algorithm generate an MST on group centres and define as filaments the structures left over after removing excessively lengthy edges. The next step is defining tendrils as the remaining unbroken chain after removing galaxies near filaments and generating MST on unassociated galaxies. The rest of galaxies that are not in tendril or near filaments are classified as void galaxies.

1.1. Galaxy and Mass Assembly survey (GAMA)

The Galaxy and Mass Assembly (GAMA) survey is a spectroscopic galactic survey carried out with the 3.9m Anglo-Australian Telescope (AAT) using the 2dF fibre feed and AAOmega multi-object spectrograph aiming to obtain about 300 000 galaxy redshifts out to a magnitude of m_r= 19.8 mag. Here, Driver, S.P. and Hopkins, A. figure as principal

investigators in the GAMA team. The spectra were taken with 2 arcsec diameter fibre, a spectral coverage from 3700 to 8900 Å, and spectral resolution of 3.2 Å. In general, GAMA lies in the parameter space between that occupied by the very wide shallow surveys and the deep pencil beam surveys, and other recent surveys such as SDSS, UKIDS and GALEX overlap with GAMA regions. The GAMA survey spans across three equatorial fields measuring 12×5 deg^2 and two southern fields out to $m_r = 19.8$, except for G23 with a limit out to $m_i = 19.2$. These survey regions are presented in the Table 1.

Region	RA range	Dec range
G02	30.2 to 38.8	-10.25 to -3.72
G09	129.0 to 141.0	-2 to +3
G12	174.0 to 186.0	-3 to +2
G15	211.5 to 223.5	-2 to +3
G23	339.0 to 351.0	-35 to -30

Table 1: Right ascension and declination ranges for the GAMA survey regions.

The two main objectives of GAMA are to use the galaxy distribution to conduct tests of the cold dark matter (CDM) paradigm and to study the internal structure and evolution of the galaxies. GAMA is optimized to study structure on $\sim 10h^{-1}$ Mpc to $\sim 1h^{-1}$ kpc scales, which includes galaxy clusters, groups, mergers and measurements of galaxy structure such as bulges and discs.

1.2. GAMA Galaxy group catalogue

One of the major data products of GAMA is the GAMA Galaxy group catalogue (G^{3}C) (Robotham et al. 2011) providing a catalogue of 23 838 galaxy groups across three equatorial fields out to $m_r < 19.8$ mag (G09, G12 and G15), based on the spectroscopic component of the GAMA survey. The final catalog contains 73 298 galaxies out of a possible 180 979, roughly 60 per cent of all galaxies. The construction of groups is generated using galaxy-galaxy linking via a friends-of-friends (FoF) algorithm (the halo-galaxy grouping is found to be less successful at recovering small-mass groups). The FoF algorithm creates links between galaxies based on their separation as a measure of the local density, operating on projected and radial separations independently. This allows the algorithm to take redshift space distortions into account and provides enough information to generate secure grouping without ambiguity. At low redshifts where the projection effects are the smallest, groups are still visually strongly associated with the filaments and nodes of the larger scale cosmic structure, while at higher redshift fewer groups are found as a result of being GAMA a magnitude-limited survey. The grouping algorithm has been tested on semi-analytic derived mock catalogues and has been designed to be extremely robust to the effects of outliers and linking errors.

From the G^{3}C a sample is selected over which the large-scale structure is detected and classified. The sample selection is done such that it is as free as possible from any intrinsic bias. An important requirement is that given a sample of galaxies and groups, we should be observing every possible galaxy and group within that absolute magnitude limit. This can be solved taking into account the faintest possible galaxy that is visible in GAMA at a given redshift z, given the apparent magnitude limit of $m_r < 19.8$ mag and using the cosmological luminosity distance D_L to that object at that redshift. Given a redshift, all galaxies whose absolute magnitude is greater than this limit are discarded, then also groups that have fewer than two members remaining. After that, the cut redshift is selected so that the largest number of groups and galaxies is retained and the value is $z = 0.213$ (Alpaslan et al. 2014). The final sample after the selection for the G09, G12 and G15 regions from the GAMA survey regions out to $z = 0.213$ contains a total of 45 542 galaxies and 6000 groups across the three equatorial GAMA regions and is the one employed in Alpaslan et al. (2014) to obtain the classification of large scale structure that we are going to use in the following sections. Throughout we assume the following cosmological parameters: $H_0 = 70$ kms^{-1}Mpc^{-1}, $\Omega_M = 0.3$ and $\Omega_\Lambda = 0.7$.

2. Sample selection

2.1. GANDALF catalog construction

In this work, we use the GANDALF catalog resulted from running the v17 GAMA spectra through a modified version of the spectral analysis program GANDALF (Sarzi et al. 2006) utilising pPXF (Cappellari and Emsellem 2004). All GANDALF fits are performed using a chi-squared least-squares minimisation method, and the stellar population templates used are those of Maraston and Strömbäck (2011), which utilise the MILES stellar library (Sánchez-Blázquez et al. 2006). The accuracy with which the position and width of an emission line can be recovered depends on how much the line stands out above the noise in the stellar spectrum, which is quantified by the line amplitude-over-noise ratio, AON. In the limit of purely statistical fluctuations the line fluxes are subject to larger errors in spectra of higher quality, although the equivalent width (EW) of the lines is better estimated at these regimes, which will be used later to estimate the SFR.

We will use the following columns from the catalog in order to create the new one with information for galaxies in filaments:

- For each galaxy: the filename, CATA Index value as provided in the spectra files, right ascension and declination for equatorial coordinates and spectroscopy redshift.
- For each emission line considered (Hβ, [OIII]λ5007, Hα and [NII]λ6583) GANDALF provides the fluxes and flux errors with applied k-correction and corrected for stellar absorption, equivalent width and amplitude-over-noise.

The measured fluxes are calculated as:

$$F_i = A_i \sqrt{2\pi}\sigma\lambda \exp(v/c)/c, \tag{1}$$

with A_i, σ and v the emission line amplitude, dispersion and recessional velocity. We start working with galaxies satisfying the filter condition given by an AON > 3 for Hα, [OIII]λ5007 and [NII]λ6583 emission lines and a less restrictive condition given by AON > 2 for Hβ.

In order to obtain the rest of required parameters for estimating the star formation rate, we use another catalog for stellar masses, restframe photometry and other stellar population parameters done by Taylor et al. (2011). The data provided is derived through stellar population synthesis modelling of broadband photometry, assuming a Chabrier initial mass function (IMF) and the Calzetti et al. (2000) dust curve. As a example we present in Figure 2 the spectra of one galaxy with $\log(M_{star}/M_{\odot}) = 10.5$ that belong to our GANDALF catalogue. The match is done in TOPCAT according to the CATAID and retaining the values of the r-band absolute magnitude M_r, stellar masses (refered to the total mass of all luminous material at the time of observation) and the distances z derived using the Tonry et al. (2000) flow model for very low redshifts. Because of the match we end up having 192 543 galaxies from an initial number of 299 200.

2.2. BPT diagram

In order to distinguish purely star-forming galaxies (SF) from galaxies hosting an AGN Baldwin et al. (1981) proposed a diagnostic diagram for emission-line galaxies based on the [OIII]λ5007/Hβ, [NII]λ6583/Hα flux ratio. The so called BPT diagram uses strong optical lines of close proximity in the ratios, limiting reddening and spectrophotometric effects, and is able to distinguish different classes of ionization. From photoionization models, the [OIII]λ5007/Hβ ratio is a tracer of the ionization level and the gas temperature, whereas [NII]λ6583/Hα traces the strength of the ionizing radiation. These diagnostic diagrams were later explored on detail by Kauffmann et al. (2003) and Kewley et al. (2001) by proposing the following curves:

$$\log([OIII]\lambda 5007/H\beta) = \frac{0.61}{\log([NII]\lambda 6583/H\alpha) - 0.05} + 1.3, \tag{2}$$

$$\log([OIII]\lambda 5007/H\beta) = \frac{0.61}{\log([NII]\lambda 6583/H\alpha) - 0.47} + 1.19. \tag{3}$$

Galaxies located between the two curves are composites (C), having mixed SF and AGN contributions, taking into account that stellar formation and AGN coexist. We show in Figure 3 the BPT diagram resulted from disposing our galaxy data between these limiting curves: below the red dashed Kaufmann curve there are the emission-line galaxies due to

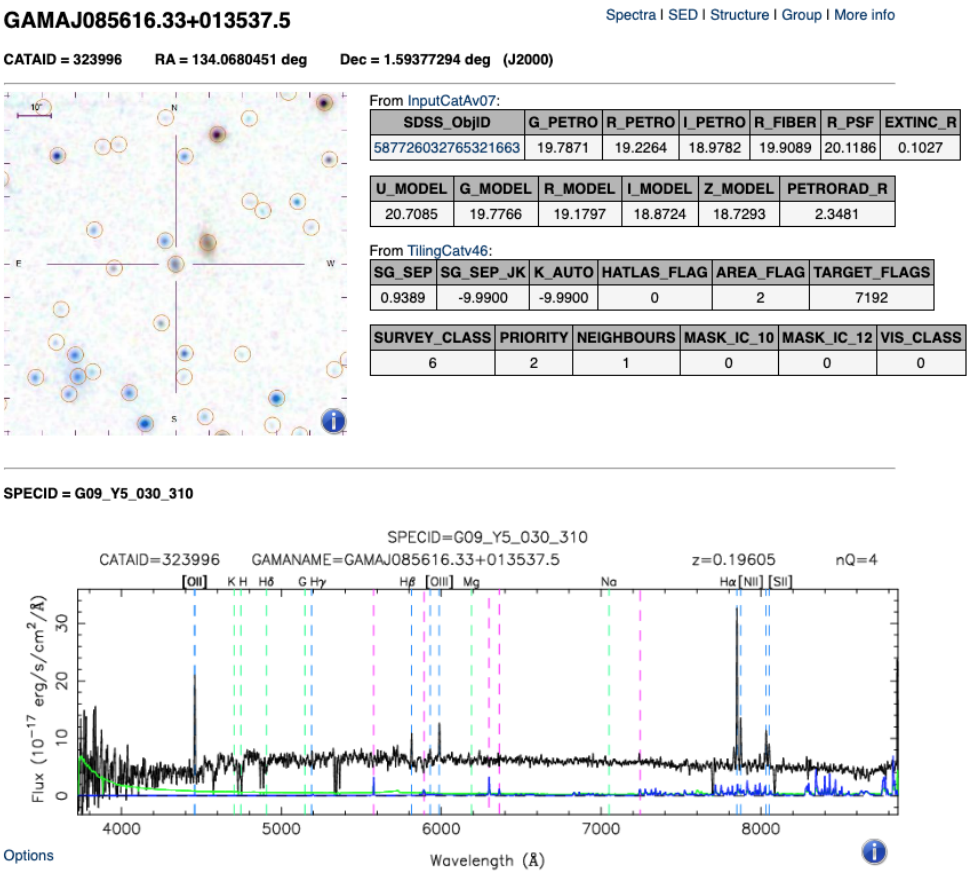


Figure 2: Example spectra for a galaxy with $\log(M_{star}/M_{\odot}) = 10.5$ from the GANDALF catalogue and their associated measurements, CATAID and equatorial coordinates.

star formation activity typical from HII regions, and over the blue dashed Kewley curve the region associated to AGN phenomenon. There is another extra dashed line in black separating Seyfert galaxies from LINERS (Low Ionization Nuclear Emission-line Regions), located in the region for low ionization level but high hardness in the ionization source. LINERS galaxies are very common (approximately one of three galaxies in the local universe are classified as LINER) and they are characterised by narrower lines in comparison with Seyfert emission lines. In our case we focus on SF galaxies, which from Table 2 result in a number of 12476 galaxies. During the process of calculation of the flux ratios we have lost a total of 3522 galaxies due to removing null values.

Classification	Number
Star Forming galaxies (SF)	12476
Composite (C)	2119
Active Galactive Nucleus (AGN)	1426

Table 2: BPT Classification of galaxies using the GANDALF catalogue.

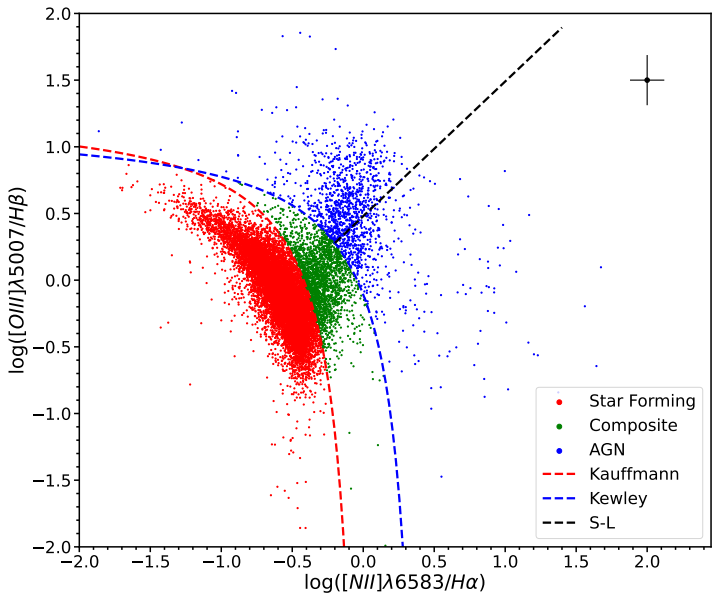


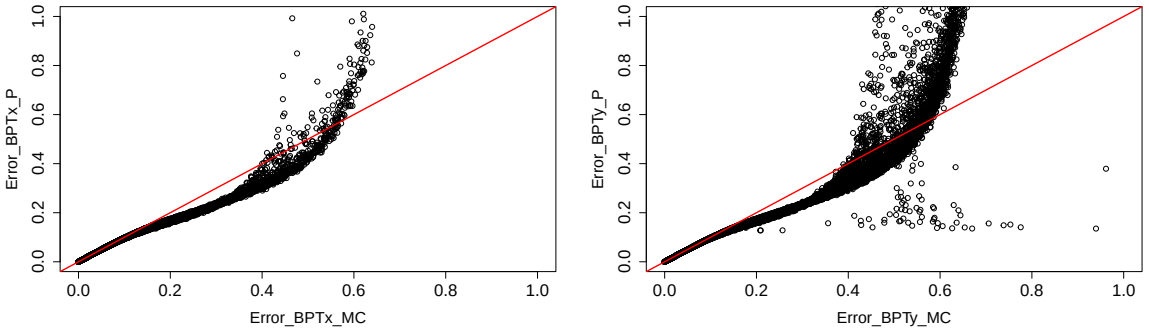
Figure 3: BPT (Baldwin et al. 1981) diagram for emission-line galaxies for the GANDALF catalogue to distinguish HII regions from AGNs or Composites based on the [OIII]λ5007/Hβ, [NII]λ6583/Hα flux ratios.

2.3. Errors estimation for the flux ratios used in the BPT diagram

Markov Chain Monte Carlo (MCMC) is probably the most popular way for the simulation of a particular distribution. The *R* package `propagate` provides a general function for the calculation of uncertainty propagation by simultaneously first and second order Taylor expansion and Monte Carlo simulation including covariances. Input data includes an expression, in our case given by the logarithm of flux ratios, a dataframe containing their standard deviations and the number of Monte Carlo simulations to be performed with a minimum of 10 000. Monte Carlo simulation is conducted using simulated data for each variable with $n =$ `nsim` samples generated from a t-distribution $X_{m,n} \sim t(\mu, \Sigma, \nu)$ using means μ_i and covariance matriz Σ constructed from the standard deviations σ_i of each variable. Each row of the simulated dataset is then evaluated with the input expression, $y_i = f(x_{m,i})$ and on the resulting y, summatory statistics such as mean, standard deviation or median are calculated.

For the calculation of errors in the BPT diagram variables we use as input expression $\log(x/y)$ for each one. The outcome of mean error calculated through Monte Carlo simulations is ~ 0.12 and ~ 0.25 for the abscissa and vertical coordinate respectively, which are the ones used in the BPT diagram in Figure 3. The results for errors estimated through Monte Carlo simulation versus propagation are shown in Figure 4 for each variable and summa-

rized in Table 3. It can be seen that initially Taylor expansion works well but as errors become larger this method offers results above red diagonal line, greatly overestimating errors. These plots together with the obtaining of greater mean values justify the choice of MCMC as method for estimating errors.



(a) Errors for x

(b) Errors for y

Figure 4: Comparison of errors estimation through propagation via Taylor expansion and Monte Carlo simulations for both flux ratios in x variable, [NII]λ6583/Hα, and y variable, [OIII]λ5007/Hβ in the BPT diagram.

Statistic	x errors (MC)	x errors (P)	y errors (MC)	y errors (P)
Median	0.08	0.08	0.19	0.16
Mean	0.12	46.04	0.25	-

Table 3: Summary statistics for the estimated errors in x variable, [NII]λ6583/Hα, and y variable, [OIII]λ5007/Hβ in the BPT diagram.

2.4. Selection effects

Many effects, related either to the position of our galaxy in the Universe, to natural limitations or to detector related issues, introduce systematic biases that have to be taken into account when analyzing our data from surveys. The most known selection effect is the Malmquist (1922) bias: due to the nature of astronomical observation we tend to pick up a relatively larger fraction of intrinsically bright objects as distance and volume increases. The mean values of absolute magnitudes, M, are biased because bright objects are oversampled and we are losing fainter sources as distance increases. As a consequence, intrinsic unrelated properties will appear to correlate because of their mutual correlation with distance.

One way of correcting the Malmquist bias is working with volume-limited samples, with a cut-off in the absolute magnitude and the distance where all the galaxies are detected so that it is achieved the completeness of the sample. Another method consists in estimating the

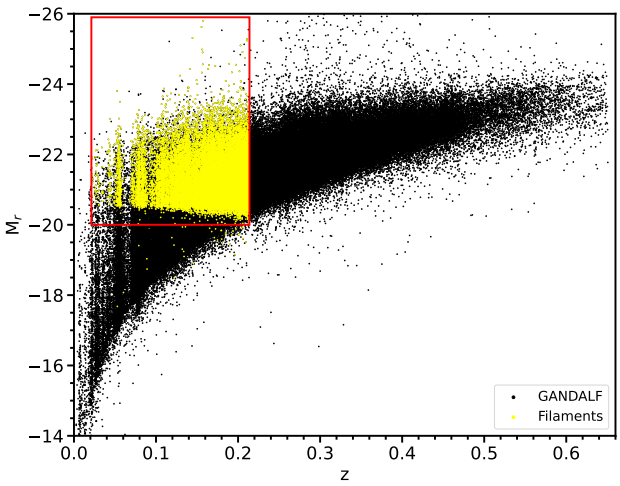


Figure 5: Redshift versus Petrosian r-band absolute magnitude (M_r) for the entire sample of GANDALF and the part of filaments. The red box correspond to the volume-limited sample given by the cut-off maximum value of the absolute magnitude for filaments.

maximum volumes V_{max} within each object could be detected and weighting each galaxy by $1/V_{max}$, correcting this way the relative counts of galaxies. This method assumes a constant space density, so is not a good approximation for nearby samples. We will apply the first method over our sample considering as cut-off in the absolute magnitude M_r the limit given by the filaments catalog which we stablish as $M_r = -20$. The result is shown in Figure 5, first for the entire sample of filaments in GANDALF and then this filter will be applied for the subsequent samples.

2.5. Filaments and control sample

The next step to create our control sample will be doing a match in TOPCAT between the previous GANDALF catalogue and the new one of filaments done by Alpaslan et al. (2014). The filaments catalog offers the identification of large scale structure in the GAMA II equatorial regions out to $z = 0.213$, classifying galaxies as belonging to filaments or tendrils, or as being void galaxies. Tendrils are detected as a second pass after the creation of filaments through a minimal spanning tree with the remaining galaxies. Then, the final left over galaxies obtain classification as void. In catalogues all galaxies are identified by unique IDs referred to the filament, tendril or void structure which appear in their corresponding catalogue. We have different catalogues for filaments providing us their properties such as the number of branches and groups that the filament has, as well as information relative to the construction of filaments. We will use the catalogue where is given the CATAID and comoving cartesian coordinates of all galaxies that are within 4.64 Mpc/h of filaments along with its ID. With this catalogue we do previously an intermediate match with the catalogue

`DistanceFrames` using as algorithm for the match criteria *exact value* for the CATAID. By this way we obtain right ascension and declination for each object that is going to be used for the next match with our previous GANDALF catalogue using as algorithm *sky* with limit value for maximum error of 1 arcsec. As a result of this match, we end up having 27 510 galaxies from an initial total number of 29 247 in the `FilGalsv02` catalogue.

The control sample will be constructed doing the match preserving the galaxies from GANDALF catalogue that have no filament association but removing the ones belonging to groups. Then, match selection in TOPCAT is *best match, symmetric* and as join type the option *1 not 2*. In this case, from 192 543 galaxies we end up having 13 122 field galaxies.

3. Star Formation Rate (SFR)

One key feature of galaxies is the process of gas conversion into stars: the mechanisms for which the cold and dense molecular clouds stop being in equilibrium and start forming stars, the time scales referred to it or the efficiency of this process are a matter of importance in astrophysics. This aspect is quantified by the Star Formation Rate (SFR), which is a measure of the rate at which star formation takes place from gas content $\frac{dM_*}{dt}$ in units of $M_\odot$/yr. From this quantity it is also defined the specific star formation rate (sSFR) dividing SFR by the stellar mass, sSFR= $\frac{\mathrm{SFR}}{M_*}$. The inverse of sSFR gives an idea about the time scale needed to form the same stellar mass the galaxy already has, keeping constant its SFR during this time. The sSFR typically decreases with stellar mass as an indication that massive galaxies could have formed its stellar populations in early epochs (z > 1).

Two main modes of star formation are known to control the growth of galaxies: the main sequence with typical values of sSFR $\sim 0.1\mathrm{Gyr}^{-1}$ comparable to the formation of Universe time scale, associated with a relatively steady rate in disk galaxies, or intermittent in dwarfs, and a starbust mode in outliers. They show sSFR values about 10 or 100 times higher and are interpreted as driven by mergers.

We estimate SFR through tracers of young (massive) stars, applying a scaling factor to a star formation-sensitive luminosity measurement for the galaxy (Kennicutt 1998) and later estimating the total number of formed stars assuming one initial mass function (IMF). Changing the mass range or choosing a different IMF alter the values for the derived SFRs as it is discussed in Kennicutt (1998). In this work we use Hα emission as tracer, an instant SFR indicator sensitive only to short timescales and independent of the previous star formation history, in contrast to the use of UV emission which suffers from contamination of evolved stars. This emission line measures only ionizing UV luminosity based on the strong fields of radiation due to O and B stars (M > $10M_\odot$) ionizing hydrogen atoms in stellar formation regions.

3.1. Extinction and reddening estimation

The main components of the interstellar medium (ISM) and HII regions are gas and dust and affects starlight which passes through it. Dust not only absorbs UV and optical radiation and re-emits in infrarred wavelengths but also scatters light from astronomical sources. The effective losses are known as extinction and it is not uniform across the whole electromagnetic spectrum. Given a specific wavelength, the extinction A_λ is defined as the difference between the observed and intrinsic magnitude, $A_\lambda \equiv m_{obs}(\lambda) - m_{int}(\lambda)$. On the other hand, the color excess is the parameter typically used to measure reddening: $E(B-V) \equiv A_B - A_V$. We can define a function, R_V putting both effects together so that a extinction law is expressed in terms of $X(x)$:

$$R_V \equiv \frac{A_V}{E(B-V)}, \qquad X(x) = \frac{A_\lambda}{E(B-V)} = R_V \frac{A_\lambda}{A_V}, \tag{4}$$

where $x \equiv 1/\lambda$ and λ have units of μm. This extinction law depends on the chemical composition of dust and consequently on the galaxy, so many extinction laws have been proposed for different environments (starbust galaxies, the diffuse intergalactic medium, etc). The most typical law is the one proposed by Cardelli et al. (1989), assuming $R_V = 3.1$ and expressed in terms of two polynomials $a(x)$, $b(x)$ in λ^{-1} which are different according to the specific range of wavelength:

$$\frac{A_\lambda}{A_V} = a(x) + \frac{b(x)}{R_V}. \tag{5}$$

In practice, spectroscopic analysis uses the parametrization $f_\lambda = \frac{A_\lambda}{A_{H\beta}} - 1$ and the coefficient $C(H\beta)$ resulted from comparing theoretical and observed values expected for the physical conditions of temperature and density:

$$C(H\beta) = \frac{1}{f(\lambda)} \times \log \frac{F_{int}(H_i)/F_{int}(H\beta)}{F_{obs}(H_i)/F_{obs}(H\beta)}. \tag{6}$$

The typical couple for the ratio is Hα and Hβ, which is known as Balmer decrement, and assuming values of $n_e = 100\text{cm}^{-3}$ and $T_e = 10000$K for the gas and the Case B recombination from photoionization models $F_{int}(H\alpha)/F_{int}(H\beta) = 2.86$. In the end the extinction value in magnitudes and the relation between the observed flux, F_{obs}, and the corrected one, F_{corr}, correspond to:

$$A_\lambda = 2.5\,[f(\lambda) + 1]\,C(H\beta), \qquad F_{corr} = F_{obs} 10^{0.4 A_\lambda}, \tag{7}$$

and combining these expressions with equation (6) we obtain:

$$F_{corr} = F_{obs} \left[\frac{F_{obs}(H\alpha)/F_{obs}(H\beta)}{2.86} \right]^{-\frac{f(H\alpha)+1}{f(H\alpha)}}. \tag{8}$$

In this case, assumming the parametrization given by Cardelli et al. (1989), $f(H\alpha) = -0.297$ and the exponent fraction results $703/297 \approx 2.36$.

3.2. Hα Star Formation Rates

Before applying the SFR calibration to Hα luminosity, there are some issues regarding the measurement of an Hα luminosity as representative of the full emission from a galaxy, given a flux measurement from a fiber-based spectrum. These issues include corrections for obscuration, due to the intrinsic dust content of the target galaxy, and aperture corrections, to account for the emission missed owing to the fiber diameter smaller than the target galaxy. Obscuration by dust intrinsic to the Star Forming (SF) galaxies can cause significant underestimates in the emission line derived SFRs. Because all the SF galaxies have measured Hα and Hβ fluxes, the Balmer decrement can be calculated and used to estimate and correct for the obscuration. On the other hand, stellar absorption in the Balmer emission lines can cause a significant overestimation in the obscuration. For this purpose, it is typically assumed a simple constant correction for stellar absorption in the measured Balmer line EW_c, which varies from about 1Å for Sa galaxies to about 4Å for extreme late types. The assumption of a common value should be restricted only to studies of large samples where the gross characteristics of the population are being examined. The commonly assumed stellar absorption of $EW_c = 2$Å derives from a line measurement technique that involves an integration of the spectrum over a wavelength range encompassing the line. Besides the obscuration correction, the emission-line luminosities also require an aperture correction to account for the fact that only a limited amount of emission from a galaxy is detected through the diameter fiber. Finally, the stellar absorption, aperture and obscuration corrected Hα luminosity is calculated for each galaxy in units of W following the prescription of Hopkins et al. (2003):

$$L_{H_{\alpha,\mathrm{int}}} = (\mathrm{EW}_{H\alpha} + \mathrm{EW}_c) \times 10^{-0.4(M_r - 34.10)} \frac{3.0 \times 10^{18}}{[6564.61(1+z)]^2} \left(\frac{F_{H\alpha}/F_{H\beta}}{2.86} \right)^{2.36}, \tag{9}$$

where $\mathrm{EW}_{H\alpha}$ is the Hα equivalent width, M_r is the SDSS k-corrected absolute r-band Petrosian magnitude and $F_{H\alpha}/F_{H\beta}$ is the Balmer decrement. Because the stellar absorption correction is previously done in galaxies from the GANDALF catalogue, $\mathrm{EW_c}$ will be zero in our case. We are considering in equation (9) the extinction correction previously done whereas the rest of factors stand for aperture correction, which assumes that the emission measured through the fiber is characteristic of the whole galaxy and that the star formation is uniformly distributed over the galaxy. The SFR is estimated from the Hα luminosity adopting the calibration given by Kennicutt (1998) in units of $M_\odot \mathrm{yr}^{-1}$:

$$SFR_{\mathrm{H}\alpha} = \frac{L_{H_{\alpha,\mathrm{int}}} \cdot 1.53}{1.27 \times 10^{34}}, \tag{10}$$

where the factor 1.53 corresponds to the conversion from the Salpeter IMF to the Chabrier IMF.

3.3. Control sample and filaments

We start considering the control sample, given by the GANDALF catalogue without galaxies in groups as indicated in section 2.5 (in this way the sample is controlled by environment) and then it is filtered as it follows:

- Amplitude over noise restrictions: AON > 3 for [OIII]λ5007, [NII]λ6583 and Hα emission lines and AON > 2 for Hβ.
- Removal of null, infinite values in Hα, Hβ fluxes and $EW_{H\alpha}$.
- Limit in redshift: $z < 0.213$.
- Consideration of just galaxies classified as SF in order to apply equation (9).

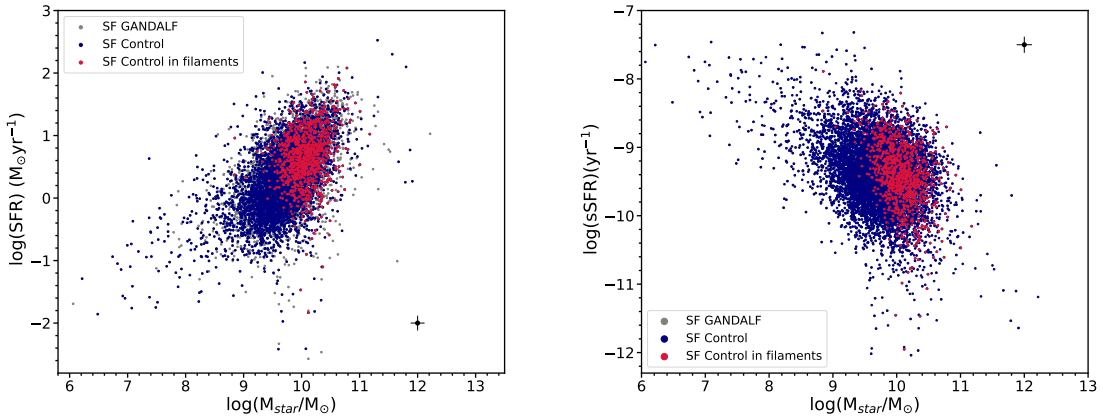
Name	Original sample	Filtered sample	Only-SF
GANDALF	192543	16021	12476
Control	119814	7311	6271
Filaments	10658	1372	1023

Table 4: Number of galaxies according to the sample and filter conditions (they are common to all samples apart from the intrinsic properties of each one as in the case for filament or control sample given by its definition).

On the other hand, the filament sample is constructed following the same prescriptions but considering previously the condition of filament. In Table 4 we include the different samples considered and the number of galaxies related to them. During our analysis we keep the GANDALF sample constructed with the same filters but considering all SF galaxies, including the ones belonging to groups (SF GANDALF). Figures 6a and 6b show the obtained results for SFR and sSFR for the SF GANDALF sample (as background in grey), SF control (blue) and SF filaments sample (red). In general the trend is the expected for SFR as increasing with the stellar mass (Brinchmann et al. 2004, Salim et al. 2005) and the opposite for the sSFR. This magnitude accounts for intrinsic star formation processes and the more massive a galaxy is the greater it is its time scale, 1/sSFR, required to form its mass. If we look at the contrast control-filaments sample we could note that for a specific value of SFR, the filaments sample exhibits a greater mass value, or the reverse if we consider a fixed value of mass: they seem to arrange around higher values of SFR and star masses. The same happens when we consider the normalized density histograms in Figures 7a, 7b, 7c: SF GANDALF and control sample almost overlap whereas the filaments sample appears displaced to higher values of SFR and stellar masses by a mean difference of ~ 0.34 in SFR.

An explanation for this behaviour could be due to the effect of environment, since mergers and typical processes of galaxies interactions occur in denser environments affecting their SFRs and sSFRs. Nevertheless, we cannot take this as an actual trend, first we have to correct our sample from the Malmquist bias, as it is explained in section 2.4.

Since we center on studying the SFR distributions we include their associated statistics only in Table 5, where it can be reflected quantitatively the effects mentioned. The presented errors correspond to the standard errors, functions of the sample size. During the process of creating the density histograms, we discovered the existence of a group of outliers associated with $M_r = -99$ and $\log(M_{star}/M_\odot) = -99$ values, so we have also removed these galaxies from our sample.



(a) SFR (b) sSFR

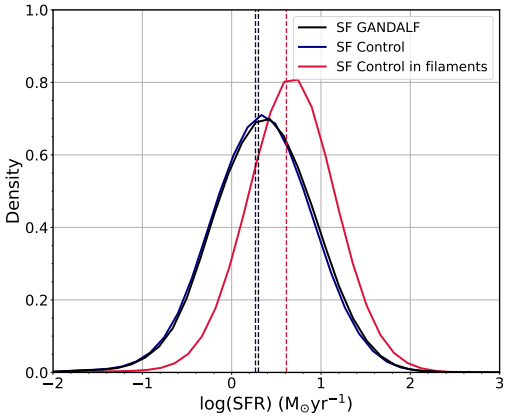
Figure 6: Stellar masses versus Star Formation Rates and Specific Star Formation Rates for SF GANDALF, SF control and filaments sample.

Statistic	SF GANDALF	SF Control	SF Filaments
Mean	0.300 ± 0.012	0.267 ± 0.015	0.61 ± 0.03
Variance	1.271 ± 0.010	1.384 ± 0.010	1.170 ± 0.009
Skewness	−12.768 ± 0.020	−12.991 ± 0.020	−18.254 ± 0.020
Kurtosis	237.2 ± 0.3	238.4 ± 0.3	432.0 ± 0.3

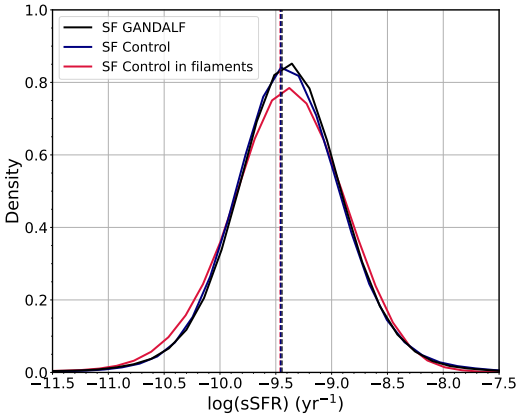
Table 5: Statistics of the SFR distribution for the different samples.

3.4. Volume limited subsample (V1) and filaments

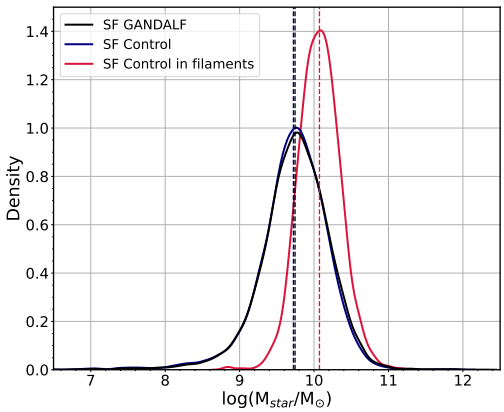
We apply the correction to the Malmquist bias by making a cut in the absolute r-band magnitude, $M_r < -20$, to the previous control sample and from this point on we work with the volume limited subsample, V1. In Table 6 we include the final number for the sample



(a) Density histogram of the SFR



(b) Density histogram of the sSFR



(c) Density histogram of the $M_{\rm star}$

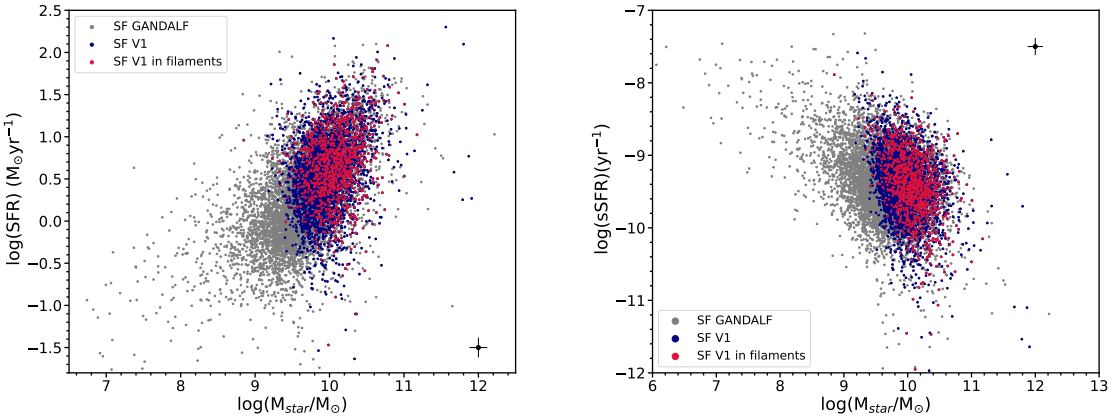
Figure 7: Density histogram of the SFR, sSFR and star mass for the different samples: SF GANDALF (black), SF control (blue) and SF filaments sample (red).

once all filters and corrections are applied, where SF GANDALF is kept without the cut in M_r. Figures 8a and 8b show the obtained results for SFR and sSFR when considering V1 sample, as well as Figures 9a, 9b and 9c display the corresponding density histograms for the magnitudes of SFR, sSFR and stellar masses. In general, the differences seem to dissappear as it is also quantitatively demonstrated in statistics in Table 7: the distributions are nearly similar although in both the SFR and star masses the filaments sample keeps taking the greatest values.

Next we center on the SFR and due to its observed correlation with the stellar mass we apply weighted on errors linear regression for SF GANDALF sample in order to obtain a fit in the way $y = ax + b$ and obtain as a result $a = 0.628 \pm 0.010$ and $b = -5.76 \pm 0.09$. Because considering subsamples (control, V1) affects the represented scaling relationships

Name	Final number
SF GANDALF	9686
SF V1	3776
SF V1 in filaments	1021

Table 6: Number of galaxies according to the sample and filter conditions.



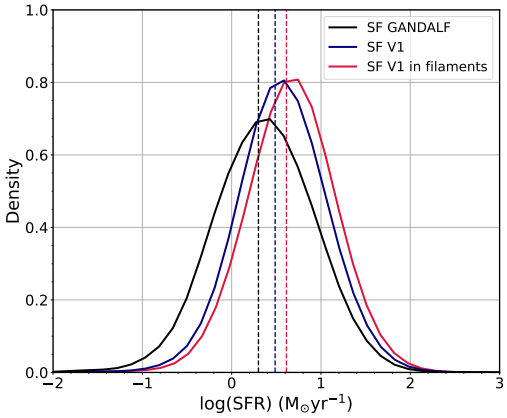
(a) SFR (b) sSFR

Figure 8: Stellar masses versus Star Formation Rates and Specific Star Formation Rates for SF GANDALF, SF V1 and SF V1 in filaments sample.

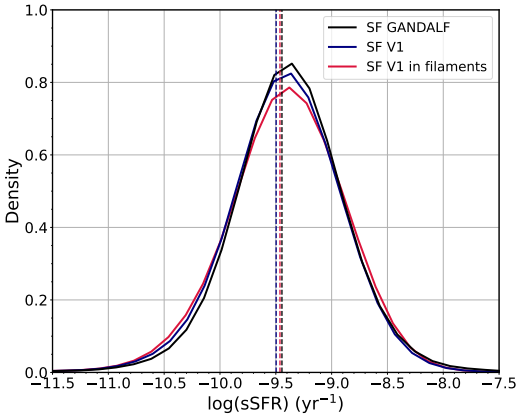
Statistic	SF GANDALF	SF V1	SF V1 in filaments
Mean	0.300 ± 0.012	0.487 ± 0.020	0.61 ± 0.03
Variance	1.271 ± 0.010	1.458 ± 0.011	1.172 ± 0.010
Skewness	−12.768 ± 0.021	−13.649 ± 0.021	−18.240 ± 0.021
Kurtosis	237.2 ± 0.3	245.1 ± 0.3	431.3 ± 0.3

Table 7: Statistics of the SFR distribution for the different samples.

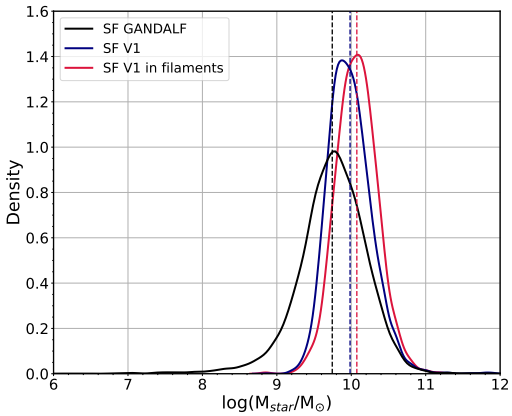
M-SFR we control for this effect keeping the slope a from this fit using all SF GANDALF galaxies, so that for the control and filaments sample we do a fit just for the ordinate b. The zero point adjustments using a least squares method for minimization for both the control and volume limited sample against filaments can be found in Table 8 . The errors of the process are computed as $S = \sqrt{\sum(y_s - y_f)^2/n - 1}$, where y_s and y_f stands for sample and fit values. We are interested in computing the difference between the zero points, Δb, of both linear fits (control, V1 versus filaments) so that obtaining a positive value represents an enhancement of SFR in galaxies belonging to filaments with respect to the control/V1 sample. Starting from the SF control sample Δb is about 0.108 dex, when we take into consideration the Malmquist bias and work with the volume limited sample, the



(a) Density histogram of the SFR



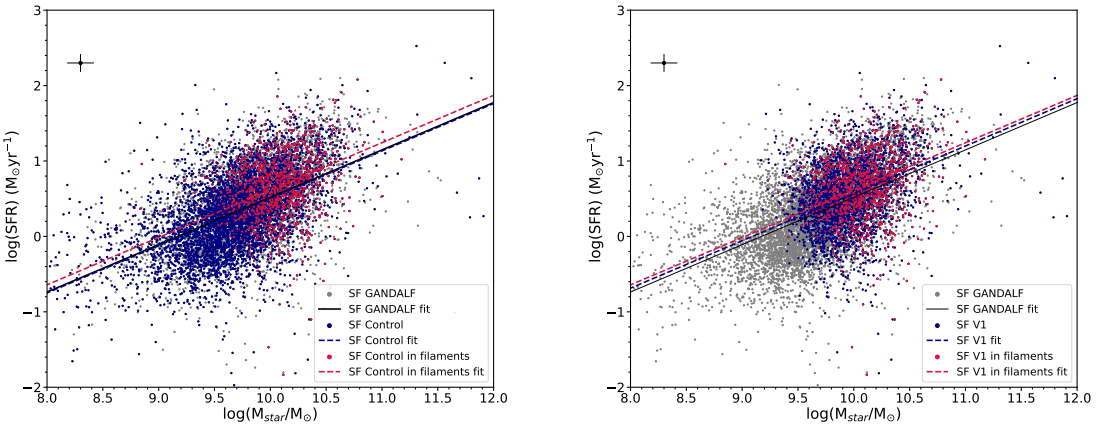
(b) Density histogram of the sSFR



(c) Density histogram of the $M_{\rm star}$

Figure 9: Density histogram of the SFR, sSFR and star mass for the different samples: SF GANDALF (black), SF V1 (blue) and SF V1 in filaments sample (red).

obtained difference about 0.042 dex becomes smaller but statistically significant. In any case, both linear fits throw a SFR enhancement for filaments. This is consistent with a scenario where denser environments induces gas inflows that enhances the SFR, although in the end the associated efficiency depends on the properties of each galaxy. Previous studies have analyzed properties of galaxies according to its belonging to large scale structures (Garduño et al. 2021, Sotillo-Ramos et al. 2021) and obtained SFR enhancements in the order of magnitude.



(a) Control and filaments sample fits

(b) V1 and filaments sample fits

Figure 10: Lineal fit for M-SFR relation for SF GANDALF, filaments, control (a) and V1 (b) sample.

Sample	**b**	**Δ b**
SF control	−5.775 ± 0.006	0.108 ± 0.020
SF control in filaments	−5.667 ± 0.014	
SF V1	−5.710 ± 0.008	0.042 ± 0.022
SF V1 in filaments	−5.668 ± 0.014	

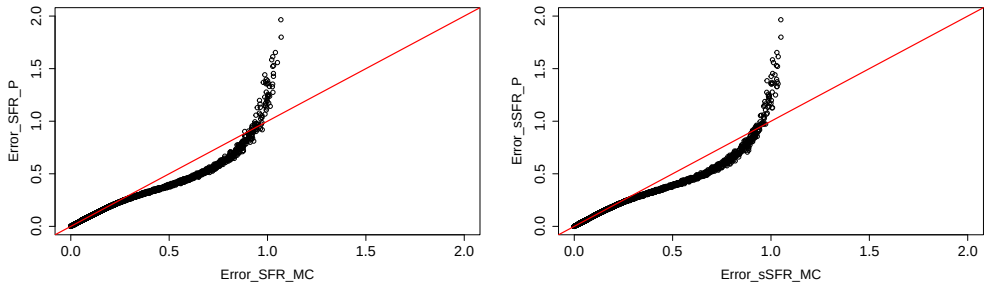
Table 8: Results for the fit to the zero point, b, keeping fixed the slope of the lineal fit for the SF GANDALF sample and derived values for the SFR enhancement, Δb.

3.5. Errors estimation for the SFR, sSFR

For the calculation of SFR and sSFR errors we proceed the same way we did in section 2.3 applying the MCMC method using R. In this case we have just considered errors for the Hα fluxes in equation (10) because they are the more relevant. The comparison between the estimated errors through Taylor expansion and the ones derived from Monte Carlo simulation is presented in Figures 11a and 11b for the SFR and sSFR. As previously mentioned, it can be seen from the red diagonal line that errors calculated through propagation make bigger as errors grow, for that reason we use the ones estimated through MCMC. In Table 9 we include the summary for these errors when they are calculated through MCMC method and propagation for comparison.

Statistic	SFR errors (MC)	SFR errors (P)	sSFR errors (MC)	sSFR errors (P)
Median	0.12	0.12	0.12	0.12
Mean	0.18	14.33	0.18	14.33

Table 9: Summary statistics for the estimated errors in SFR and sSFR through MCMC method and propagation via Taylor expansion.



(a) SFR errors

(b) sSFR errors

Figure 11: Comparison of errors estimation through propagation via Taylor expansion and Monte Carlo simulations for the SFR and sSFR.

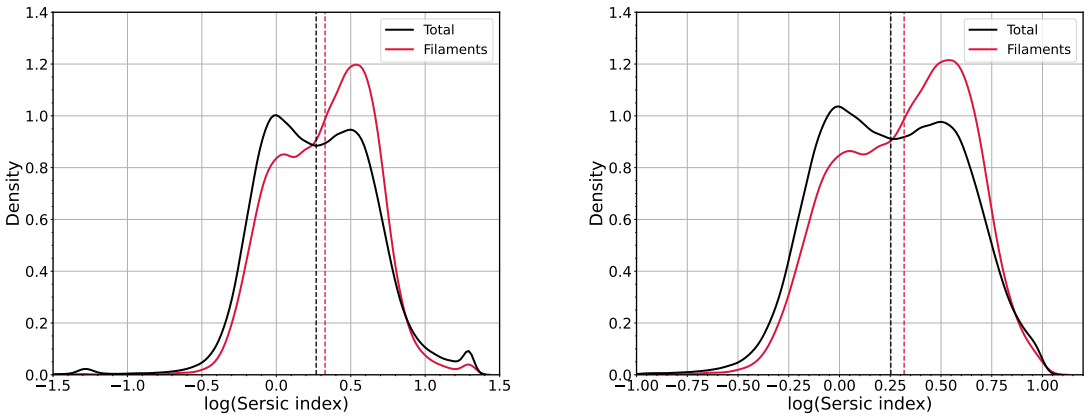
4. Morphology

The shapes and sizes of galaxies are defined by the orbital motions of their constituent stellar populations, so they relate to the stellar formation history and processes involving collapse, merging, infall and feedback. As a result, the environment (filament, void, groups, etc.) has an influence in global galaxy parameters such as colour, concentration or size. There is the well-known morphology-density relation (Dressler 1980) indicating the preference of early type galaxies for dense environments of galaxy groups and clusters. Kelvin et al. (2012) estimate the Sersic indexes for galaxies modelled independently in the *ugrizYJHK* bandpasses. They utilize Structural Investigation of Galaxies via Model Analysis (SIGMA), an automated code designed to produce single-Sersic and multicomponent profile fits for galaxies in the GAMA data set. SIGMA uses a wide-range of image analysis software and handlers to perform bulk structural analysis on an input catalogue of galaxies. In this process the software GALFIT is key, which is able to create a realistic model of each input galaxy by fitting one or more analytical functions in multiple combinations. Among the available fitting functions is the Sersic profile (Sérsic 1963) which describes how the intensity I varies as a function of radius r:

$$I(r) = I_e \exp\left[-b_n\left((\frac{r}{r_e})^{1/n} - 1\right)\right], \tag{11}$$

where I_e is the intensity at the effective radius r_e (the radius containing the half of the total light), n is the Sersic index and b_n is a function of Sersic index. Different values of the index parameter n allows to model a wide range of galaxy light profiles: $n = 1$ gives an exponential profiles suitable for galactic discs and $n = 4$ offers a Vaucouleurs profile typically associated with massive spheroidal components such as bulges or elliptical galaxies.

The catalogue `SersicCatAllv07` (Kelvin et al. 2012) provides information about morphology of the galaxies in our sample. It contains the output result of using SIGMA v0.9-0 to generate a single-Sersic fit to every GAMA object. Some of the output parameters given in the catalogue for different photometric bands are: type of fit, number of GALFIT runs required, GALFIT run result, reduced chi-squared of output model, Sersic index or ellipticity. Although there is no explicit constraints on the range of acceptable Sersic indexes, GALFIT has internal limits of $0.05 < n < 20$ but obtained Sersic parameters peak primarily in the range $0.2 < n < 10$. Peaks at the extremes previously mentioned arise due to failed fits for which the fitting procedure drifted into an unrealistic parameter space during the minimization routine. In our work we use the analysis and modelling obtained in the r-band. As a result of this new match between catalogues, using right ascension and declination as criteria, there are 150 768 galaxies remaining from the initial GANDALF sample.



(a) (b)

Figure 12: Density histograms of the Sersic index for the total GANDALF catalogue (black line) and the filaments sample (red line). The dashed vertical lines indicate the mean of each sample.

Figure 12 shows the density distribution for r-band Sersic indexes colored in black for galaxies in the GANDALF catalogue and in red for filament sample. In Figure 12b we plot the density distribution removing values associated with failed fits which appear as additional peaks at extremes in 12a. Both samples appear bimodal, consisting of two approximately Gaussian-like distributions whose means are $n \sim 1$ and ~ 3.5. These two peaks correspond

to the two main galaxy morphologies: late-type disc dominated galaxies for $n = 1$ and early-type spheroidal gaslaxies for $n = 3.5$. Actually, there is a rough separation at $n \approx 1.9$ for the r-band between early and late type galaxies. Based on the Sersic index and this limit, 53 percent of the GANDALF sample correspond to late-type galaxies whereas 57 percent of the filament sample correspond to early-type galaxies.

4.1. Control and V1 samples versus filaments

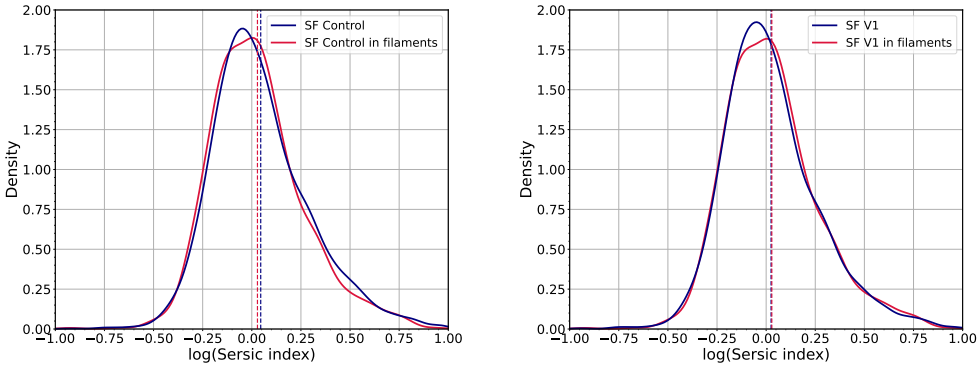
We do the match between the Sersic Index catalogue and the GANDALF catalogue obtained from removing galaxies in groups, which is the control sample as described in section 3.3. Because of the match done by the algorithm of sky using right ascension and declination with an error of 1 arcsec, we end up having 92 097 galaxies. Among them, 5846 galaxies belong to the SF control sample and 991 galaxies are in filaments. The same procedure is applied to the volume limitad sample (V1) considering the filtering condition given by M_r and the resulting density histograms are shown in Figures 13a and 13b, with the associated statistics in Table 10.

From the results, in both cases (control and volume limited samples) the bimodal features of the distribution are lost. Removing galaxies in groups have the effect of making similar the distributions in Sersic index. This can also be seen from the obtained statistics and the effect is even bigger when the volume limited sample is considered, in this case the mean values are almost the same. According to the mentioned frontier at n for the r-band, both filaments and SF control sample exhibit the majority of their galaxies belonging to the late-type (83.4 percent of the SF control sample and 85.9 for the filaments). The same happens when we look at the V1 sample, 85.9 percent of it and 85.8 of the filaments sample correspond to late-type galaxies. We could explain these results as a consequence of filtering for SF galaxies, so that we are removing the early type galaxies contribution in the bimodal original distribution that could possibly have a composite or AGN classification in the BPT diagnosis.

Statistic	**GANDALF**	**Filaments**
Mean	0.2678 ± 0.0010	0.3276 ± 0.0021
Variance	0.1377 ± 0.0010	0.1053 ± 0.0008
Skewness	−0.157 ± 0.006	−0.183 ± 0.006
Kurtosis	1.09 ± 0.16	0.17 ± 0.16

Statistic	**SF Control**	**SF Filaments**	**SF V1**
Mean	0.045 ± 0.003	0.029 ± 0.007	0.025 ± 0.004
Variance	0.061 ± 0.003	0.055 ± 0.003	0.057 ± 0.004
Skewness	0.66 ± 0.03	0.64 ± 0.03	0.64 ± 0.04
Kurtosis	0.8 ± 0.4	0.9 ± 0.4	1.0 ± 0.4

Table 10: Statistics of the log(Sersic index) distribution for the different samples.



(a) Control and filaments sample

(b) V1 and filaments sample

Figure 13: Density histograms of the Sersic index for the filaments sample in red, in blue the SF control sample (a) and the SF V1 sample (b).

5. Summary and conclusions

We have analyzed a key parameter in the understanding of galaxy evolution as it is the SFR, and additionally the morphology for three different samples against filaments galaxies in order to study the possible effect of the environment. GAMA survey and its catalog products such as GANDALF, the GAMA Galaxy group catalogue (G^3C), and the filaments catalogue, have allowed us to access the large scale structure in galaxies from the three equatorial GAMA fields.

Starting with these catalogues, we have applied different filter conditions, including those associated to remove galaxies with an AGN (BPT diagram), and the others derived from observational and selection effects, such as the dust extinction or the Malmquist bias. After all this discrimination, we end up with three different samples: SF GANDALF, SF Control and the volume limited sample, SF V1, to control for environment and selection effects. We compare them with filaments through density histograms, M-SFR, M-sSFR relations and offsets in the zero point fit to the M-SFR relation. The errors estimation of calculated magnitudes have been considered by means of Monte Carlo simulations after comparing with errors obtained through Taylor expansion, and confirming that they progressively rise as Monte Carlo errors grow. Apart from Monte Carlo simulations that have been done using the library *propagate* from *R* software package, all these results have been developed on *Jupyter Notebook* and would be shared with any interested reader if requested. Our main conclusions can be given in the following bullet points:

- Overall, when considering the complete GANDALF and filaments catalog, differences in morphology come out: although both samples show bimodal distributions in Sersic index, there is a 3% of excess in GANDALF galaxies that can be classified as late-type

galaxies, and the contrary in filaments galaxies, in a 7%.

- Higher Sersic indexes together with the M-SFR, M-sSFR relation for the control sample could possible make us expect more massive galaxies in filaments given a SFR value (or the other way around) as well as lower values for sSFR, which would be coherent with early-type galaxies. Nevertheless, these morphological differences disappear when we work with the control sample, even more when it is the volume limited sample. Taking into account that in these samples we have filtered for SF galaxies, we could attribute this effect to the presence of AGN and composite galaxies in the original complete catalogues.

- We have identified a selection effect when plotting the M-SFR and M-sSFR relations and demonstrated the importance of working with a volume limited sample. As it can be seen from density histograms, the environmental differences decreased. The obtained SFR enhancement, given by the zero point offset for the volume limited sample, is reduced by $\sim$ 0.066 dex, but is still statistically significant taking into account its logarithmic nature and the high numbers of galaxies that compound the samples.

- In both cases the zero point offset keeps being positive for the filaments over the control and volume limited samples, suggesting that mechanisms enhancing SFR should be dominant in SF filament galaxies.

6. Future work

Following the path of previous works studying galaxy properties affected by their environment using GAMA data and their large scale structure classification (e.g., Garduño et al. 2021, Sotillo-Ramos et al. 2021), the next step would be to consider a stricter control sample obtained by finding matches in stellar mass between our filament galaxies and volume limited sample. This methodology ensures small bias when finding differences in galaxy properties. Another point would be make a comparison between our results and simulations, although it would previously require to extend the large scale structure classification as filaments to known simulations, e.g., the ILLUSTRIS simulation.

References

M. Alpaslan, A. S. G. Robotham, S. Driver, P. Norberg, I. Baldry, A. E. Bauer, J. Bland-Hawthorn, M. Brown, M. Cluver, M. Colless, C. Foster, A. Hopkins, E. Van Kampen, L. Kelvin, M. A. Lara-Lopez, J. Liske, A. R. Lopez-Sanchez, J. Loveday, T. McNaught-Roberts, A. Merson, and K. Pimbblet. Galaxy And Mass Assembly (GAMA): the large-scale structure of galaxies and comparison to mock universes. , 438(1):177–194, Feb. 2014. doi: 10.1093/mnras/stt2136.

V. Avila-Reese. Understanding Galaxy Formation and Evolution. In *Solar, Stellar and Galactic Connections Between Particle Physics and Astrophysics*, volume 2 of *Astrophysics and Space Science Proceedings*, page 115, Jan. 2007. doi: 10.1007/978-1-4020-5575-1_4.

J. A. Baldwin, M. M. Phillips, and R. Terlevich. Classification parameters for the emission-line spectra of extragalactic objects. , 93:5–19, Feb. 1981. doi: 10.1086/130766.

J. Brinchmann, S. Charlot, S. D. M. White, C. Tremonti, G. Kauffmann, T. Heckman, and J. Brinkmann. The physical properties of star-forming galaxies in the low-redshift Universe. , 351(4):1151–1179, July 2004. doi: 10.1111/j.1365-2966.2004.07881.x.

D. Calzetti, L. Armus, R. C. Bohlin, A. L. Kinney, J. Koornneef, and T. Storchi-Bergmann. The Dust Content and Opacity of Actively Star-forming Galaxies. , 533(2):682–695, Apr. 2000. doi: 10.1086/308692.

M. Cappellari and E. Emsellem. Parametric Recovery of Line-of-Sight Velocity Distributions from Absorption-Line Spectra of Galaxies via Penalized Likelihood. , 116(816):138–147, Feb. 2004. doi: 10.1086/381875.

J. A. Cardelli, G. C. Clayton, and J. S. Mathis. The Relationship between Infrared, Optical, and Ultraviolet Extinction. , 345:245, Oct. 1989. doi: 10.1086/167900.

A. Dressler. Galaxy morphology in rich clusters: implications for the formation and evolution of galaxies. , 236:351–365, Mar. 1980. doi: 10.1086/157753.

L. E. Garduño, M. A. Lara-López, O. López-Cruz, A. M. Hopkins, M. S. Owers, K. A. Pimbblet, and B. W. Holwerda. Galaxy And Mass Assembly (GAMA): the interplay between galaxy mass, SFR, and heavy element abundance in paired galaxy sets. , 501(2): 2969–2982, Feb. 2021. doi: 10.1093/mnras/staa3799.

O. Hahn, C. M. Carollo, C. Porciani, and A. Dekel. The evolution of dark matter halo properties in clusters, filaments, sheets and voids. , 381(1):41–51, Oct. 2007. doi: 10.1111/j.1365-2966.2007.12249.x.

A. M. Hopkins, C. J. Miller, R. C. Nichol, A. J. Connolly, M. Bernardi, P. L. Gómez, T. Goto, C. A. Tremonti, J. Brinkmann, Ž. Ivezić, and D. Q. Lamb. Star Formation Rate Indicators in the Sloan Digital Sky Survey. , 599(2):971–991, Dec. 2003. doi: 10.1086/379608.

G. Kauffmann, T. M. Heckman, C. Tremonti, J. Brinchmann, S. Charlot, S. D. M. White, S. E. Ridgway, J. Brinkmann, M. Fukugita, P. B. Hall, Ž. Ivezić, G. T. Richards, and D. P. Schneider. The host galaxies of active galactic nuclei. , 346(4):1055–1077, Dec. 2003. doi: 10.1111/j.1365-2966.2003.07154.x.

G. Kauffmann, S. D. M. White, T. M. Heckman, B. Ménard, J. Brinchmann, S. Charlot, C. Tremonti, and J. Brinkmann. The environmental dependence of the relations between stellar mass, structure, star formation and nuclear activity in galaxies. , 353(3):713–731, Sept. 2004. doi: 10.1111/j.1365-2966.2004.08117.x.

L. S. Kelvin, S. P. Driver, A. S. G. Robotham, D. T. Hill, M. Alpaslan, I. K. Baldry, S. P. Bamford, J. Bland-Hawthorn, S. Brough, A. W. Graham, B. Häussler, A. M. Hopkins, J. Liske, J. Loveday, P. Norberg, S. Phillipps, C. C. Popescu, M. Prescott, E. N. Taylor, and R. J. Tuffs. Galaxy And Mass Assembly (GAMA): Structural Investigation of Galaxies via Model Analysis. , 421(2):1007–1039, Apr. 2012. doi: 10.1111/j.1365-2966.2012.20355.x.

J. Kennicutt, Robert C. Star Formation in Galaxies Along the Hubble Sequence. , 36:189–232, Jan. 1998. doi: 10.1146/annurev.astro.36.1.189.

L. J. Kewley, M. A. Dopita, R. S. Sutherland, C. A. Heisler, and J. Trevena. Theoretical Modeling of Starburst Galaxies. , 556(1):121–140, July 2001. doi: 10.1086/321545.

K. G. Malmquist. On some relations in stellar statistics. *Meddelanden fran Lunds Astronomiska Observatorium Serie I*, 100:1–52, Mar. 1922.

C. Maraston and G. Strömbäck. Stellar population models at high spectral resolution. , 418 (4):2785–2811, Dec. 2011. doi: 10.1111/j.1365-2966.2011.19738.x.

A. S. G. Robotham, P. Norberg, S. P. Driver, I. K. Baldry, S. P. Bamford, A. M. Hopkins, J. Liske, J. Loveday, A. Merson, J. A. Peacock, S. Brough, E. Cameron, C. J. Conselice, S. M. Croom, C. S. Frenk, M. Gunawardhana, D. T. Hill, D. H. Jones, L. S. Kelvin, K. Kuijken, R. C. Nichol, H. R. Parkinson, K. A. Pimbblet, S. Phillipps, C. C. Popescu, M. Prescott, R. G. Sharp, W. J. Sutherland, E. N. Taylor, D. Thomas, R. J. Tuffs, E. van Kampen, and D. Wijesinghe. Galaxy and Mass Assembly (GAMA): the GAMA galaxy group catalogue (G^3Cv1). , 416(4):2640–2668, Oct. 2011. doi: 10.1111/j.1365-2966.2011.19217.x.

S. Salim, S. Charlot, R. M. Rich, D. Schiminovich, GALEX Team, and DEEP2 Team. Star Formation History in the Extended Groth Strip - Constraints from GALEX (UV) and Optical Photometry. In *American Astronomical Society Meeting Abstracts*, volume 207 of *American Astronomical Society Meeting Abstracts*, page 52.06, Dec. 2005.

P. Sánchez-Blázquez, R. F. Peletier, J. Jiménez-Vicente, N. Cardiel, A. J. Cenarro, J. Falcón-Barroso, J. Gorgas, S. Selam, and A. Vazdekis. Medium-resolution Isaac Newton Telescope library of empirical spectra. , 371(2):703–718, Sept. 2006. doi: 10.1111/j.1365-2966.2006.10699.x.

M. Sarzi, J. Falcón-Barroso, R. L. Davies, R. Bacon, M. Bureau, M. Cappellari, P. T. de Zeeuw, E. Emsellem, K. Fathi, D. Krajnović, H. Kuntschner, R. M. McDermid, and R. F. Peletier. The SAURON project - V. Integral-field emission-line kinematics of 48 elliptical and lenticular galaxies. , 366(4):1151–1200, Mar. 2006. doi: 10.1111/j.1365-2966.2005.09839.x.

J. L. Sérsic. Influence of the atmospheric and instrumental dispersion on the brightness distribution in a galaxy. *Boletin de la Asociacion Argentina de Astronomia La Plata Argentina*, 6:41–43, Feb. 1963.

R. K. Sheth and G. Tormen. On the environmental dependence of halo formation. , 350(4):1385–1390, June 2004. doi: 10.1111/j.1365-2966.2004.07733.x.

D. Sotillo-Ramos, M. A. Lara-López, A. M. Pérez-García, R. Pérez-Martínez, A. M. Hopkins, B. W. Holwerda, J. Liske, A. R. López-Sánchez, M. S. Owers, and K. A. Pimbblet. Galaxy and mass assembly (GAMA): The environmental impact on SFR and metallicity in galaxy groups. , 508(2):1817–1830, Dec. 2021. doi: 10.1093/mnras/stab2641.

M. Tanaka, T. Goto, S. Okamura, K. Shimasaku, and J. Brinkmann. The Environmental Dependence of Galaxy Properties in the Local Universe: Dependences on Luminosity, Local Density, and System Richness. , 128(6):2677–2695, Dec. 2004. doi: 10.1086/425529.

E. Taylor, A. Hopkins, I. Baldry, M. Brown, S. Driver, L. Kelvin, D. Hill, A. Robotham, J. Bland-Hawthorn, D. Jones, R. Sharp, D. Thomas, J. Liske, J. Loveday, P. Norberg, J. Peacock, S. Bamford, S. Brough, M. Colless, and D. Wijesinghe. Galaxy and mass assembly (gama): stellar mass estimates. *Monthly Notices of The Royal Astronomical Society - MON NOTIC ROY ASTRON SOC*, 418, 08 2011. doi: 10.1111/j.1365-2966.2011.19536.x.

J. L. Tonry, J. P. Blakeslee, E. A. Ajhar, and A. Dressler. The Surface Brightness Fluctuation Survey of Galaxy Distances. II. Local and Large-Scale Flows. , 530(2):625–651, Feb. 2000. doi: 10.1086/308409.